Deletion of *claudin-10* (*Cldn10*) in the thick ascending limb impairs paracellular sodium permeability and leads to hypermagnesemia and nephrocalcinosis

Tilman Breiderhoff[a,1], Nina Himmerkus[b], Marchel Stuiver[c], Kerim Mutig[d], Constanze Will[c], Iwan C. Meij[a], Sebastian Bachmann[d], Markus Bleich[b], Thomas E. Willnow[a], and Dominik Müller[c,1]

[a]Max Delbrück Center for Molecular Medicine, 13125 Berlin, Germany; [b]Institute of Physiology, Christian Albrechts University of Kiel, 24098 Kiel, Germany; [c]Department of Pediatric Nephrology, Charité Universitätsmedizin, 13353 Berlin, Germany; and [d]Institute for Vegetative Anatomy, Charité Universitätsmedizin, 10117 Berlin, Germany

In the kidney, tight junction proteins contribute to segment specific selectivity and permeability of paracellular ion transport. In the thick ascending limb (TAL) of Henle's loop, chloride is reabsorbed transcellularly, whereas sodium reabsorption takes transcellular and paracellular routes. TAL salt transport maintains the concentrating ability of the kidney and generates a transepithelial voltage that drives the reabsorption of calcium and magnesium. Thus, functionality of TAL ion transport depends strongly on the properties of the paracellular pathway. To elucidate the role of the tight junction protein claudin-10 in TAL function, we generated mice with a deletion of *Cldn10* in this segment. We show that claudin-10 determines paracellular sodium permeability, and that its loss leads to hypermagnesemia and nephrocalcinosis. In isolated perfused TAL tubules of claudin-10–deficient mice, paracellular permeability of sodium is decreased, and the relative permeability of calcium and magnesium is increased. Moreover, furosemide-inhibitable transepithelial voltage is increased, leading to a shift from paracellular sodium transport to paracellular hyperabsorption of calcium and magnesium. These data identify claudin-10 as a key factor in control of cation selectivity and transport in the TAL, and deficiency in this pathway as a cause of nephrocalcinosis.

Renal ion reabsorption is vital for bodily functions. Whereas regulation of transporters and channels involved in transcellular ion transport has been characterized in much detail, the functional and molecular determinants of paracellular ion transport in the kidney remain incompletely understood.

In the thick ascending limb (TAL) of Henle's loop, both transcellular and paracellular ion transport pathways contribute to reabsorption of Na^+, Cl^-, Mg^{2+}, and Ca^{2+}. Na^+ and Cl^- are reabsorbed mostly transcellularly by the concerted action of channels and transporters. Mutations in five of the genes involved lead to Bartter syndrome, a disorder characterized by salt wasting and polyuria (1). Whereas Cl^- is transported exclusively transcellularly, ~50% of the Na^+ load, as well as Ca^{2+} and Mg^{2+}, are reabsorbed via paracellular pathways. In the TAL, this paracellular route is highly cation-selective (2). The paracellular passage is largely controlled by the tight junction (TJ), a supramolecular structure of membrane-spanning proteins, their intracellular adapters, and scaffolding proteins (3). Claudins, a family comprising 27 members (4), are the main components of the TJ defining the permeability properties. They interact via their extracellular loops with corresponding claudins of the neighboring cell to allow or restrict passage of specific solutes (5, 6). In the kidney, their expression pattern is closely related to the corresponding segment-specific solute reabsorption profile. Several claudins are expressed in the TAL, including claudin-16, -19, -10, -3, and -18 (7–10). The importance of claudin-16 and -19 in this tissue is documented by mutations in *CLDN16* and *CLDN19*, which cause familial hypomagnesemia, hypercalciuria, and nephrocalcinosis, an autosomal recessive disorder that leads to end-stage renal disease (8, 11). The relevance of CLDN16 for paracellular reabsorption of Mg^{2+} and Ca^{2+} was confirmed in mouse models with targeted gene disruption (12–14). In addition, claudin-14, expressed in the TAL of mice on a high-calcium diet, was identified as negative regulator of claudin-16 function (15), and sequence variants in *CLDN14* have been associated with human kidney stone disease (16).

The functional significance of claudin-10, which is also expressed in the TAL, remains unclear. This TJ protein is expressed in two isoforms, claudin-10a and claudin-10b, which differ in their first extracellular loop (9, 17). In cultured epithelial cells, heterologous expression of claudin-10a increases paracellular anion transport, whereas claudin-10b expression increases paracellular cation transport. Both isoforms are expressed differentially along the nephron, with claudin-10a found predominantly in cortical segments, whereas claudin-10b is enriched in the medullary region (9, 17, 18).

In the present study we generated a mouse model with a TAL-specific *Cldn10* gene defect to query the role of this protein in renal paracellular in transport in vivo. We found that claudin-10 is crucial to paracellular Na^+ handling in the TAL, and that its absence leads to a shift from paracellular sodium transport to paracellular hyperreabsorption of Ca^{2+} and Mg^{2+}.

Results

Generation of Mice with Deletion of *Cldn10* in the TAL. Using homologous recombination in murine embryonic stem cells, we introduced loxP sites into the mouse genome flanking exons 2 and 3 of *Cldn10*, the gene encoding claudin-10 (Fig. S1). These exons are present in the splice variants *Cldn10a* and *Cldn10b* (9, 17) and their deletion is predicted to result in an premature stop codon in all encoded isoforms. Mice carrying the floxed allele were bred to mice expressing Cre recombinase under the control of the murine kidney-specific cadherin-16 promoter (*ksp-cre*[+]), resulting in recombinase activity in the TAL and more distal nephron segments (19). Mice homozygous for the floxed *Cldn10* allele (*Cldn10^{fl/fl}*) and expressing Cre (*Cldn10^{fl/fl} kspcre[+]*), termed "cKO" herein, were born at normal Mendelian ratio. They were viable and fertile, and exhibited no obvious growth defect. *Cldn10^{+/fl} kspcre[+]* and *Cldn10^{fl/fl} kspcre[−]* mice, termed "controls" herein, were phenotypically indistinguishable from *Cldn10^{+/+}* animals, excluding confounding effects of the Cre transgene or the insertion of loxP sites on renal functions.

Western blot analysis of kidney membrane extracts confirmed an almost complete absence of claudin-10 in this tissue of cKO mice (Fig. 1*A*). Loss of *Cldn10* expression in the TAL of cKOs was confirmed by quantitative PCR (qPCR) using cDNA generated from isolated nephron segments (Fig. 1*B*). In control
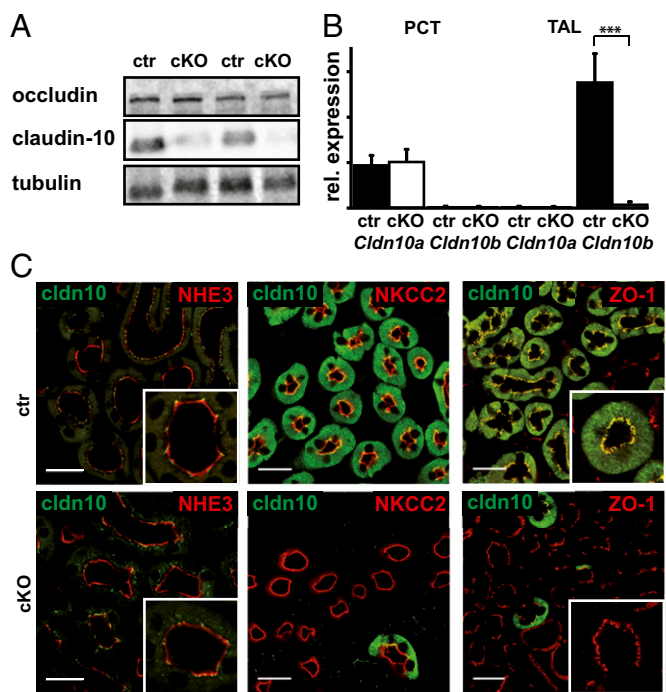
PHYSIOLOGY

Fig. 1. Analysis of claudin-10 expression in the kidney. (*A*) Western blot analysis of kidney membrane extracts from control (ctr) and cKO mice. A dramatic reduction in claudin-10 protein can be seen in kidneys of cKO mice. Levels of the TJ marker occludin are unchanged. (*B*) Gene expression analysis of *Cldn10* variants on cDNA from isolated segments of the nephron. (*C*) Immunohistological detection of claudin-10 and markers for PCT (NHE3) and TAL (NKCC2) on sections from control mice (ctr) and cKO mice demonstrates no difference in the signal for claudin-10 in the PCT between WT and cKO. Claudin-10 is expressed in TAL tubules positive for NKCC2. No specific claudin-10 staining is evident in the TAL of cKO mice. Claudin-10 is detected in TJs positive for ZO-1. This signal is absent in cKO mice, whereas ZO-1 staining is unchanged. (Scale bar: 25 µm.)

animals, *Cldn10a* transcripts were abundant in the proximal convoluted tubule (PCT), whereas *Cldn10b* predominated in the TAL. In cKO mice, levels of *Cldn10a* transcripts were unchanged in the PCT, but *Cldn10b* transcripts were virtually absent from the TAL. To confirm successful ablation of claudin-10 expression in the TAL (but not in other nephron segments), we analyzed the protein by immunofluorescence microscopy.

In control animals, claudin-10 is located mainly in the TAL, as documented by coimmunostaining with the $Na^+K^+2Cl^-$ cotransporter (NKCC2) (Fig. 1*C*). In this segment, a large portion of the claudin-10 immunofluorescence signal is located outside of the TJ; however, claudin-10 is present in the TJ, as demonstrated by colocalization with the TJ protein ZO-1. PCTs positive for the sodium-proton exchanger NHE-3 showed a considerably weaker signal restricted to the TJ area. Claudin-10 immunoreactivity is virtually absent in NKCC2-positive tubules of cKO mice, in line with the activity of Cre recombinase in this cell type. The immunoreactivity of claudin-10 in PCTs of cKOs remained unchanged, however. ZO-1 staining in TAL sections of cKOs was unchanged compared with controls, indicating no unspecific effect on TJ structures. The TJ localization of claudin-16 and claudin-19 in medullary rays was similar in cKOs and controls (Fig. S2).

Nephrocalcinosis in Claudin-10–Deficient Mice. To investigate the phenotypic consequences of renal claudin-10 deficiency, we performed a histological examination of the kidneys of 10-wk-old cKO mice and their respective controls. Kidneys from cKO mice contained extensive medullary calcium deposits, as revealed by von Kossa and alizarin red S staining (Fig. 2 *A*, *B*, and *D*). The deposits were found along the outer stripe of the outer medulla

and in the inner stripe of the outer medulla at the transition to the inner medulla. Calcification was observed in all *Cldn10^{fl/fl} kspcre^+* mice analyzed (*n* >10), but was not in control animals (*n* >10).

Hypermagnesemia in Claudin-10–Deficient Mice. The detection of extensive calcification suggests alterations in renal ion homeostasis in mice deficient for claudin-10. We confirmed this assumption by analysis of urine and serum parameters. cKO mice exhibited moderate polyuria and polydipsia (Table 1), with increased urinary volume paralleled by decreased urine osmolality. In addition, the urine of cKO mice was more acidic than that of controls (urine [H^+]: 0.5 µmol/L in controls vs. 3.2 µmol/L in cKO mice). Serum phosphate concentration was 28% higher and serum Mg^{2+} concentration was almost twofold higher in cKO mice compared with controls (Table 1). Correspondingly, in the cKO mice, the urinary fractional excretion (FE) of Mg^{2+} was only 52% of the control values. In addition, FE_{Ca}^{2+} was slightly decreased in the cKO mice, although this effect was not reflected in hypercalcemia (Table 1); on the contrary, the cKO animals had slightly decreased serum Ca^{2+} levels. The cKO mice had a 1.4-fold higher serum urea concentration and a 1.4-fold lower FE of urea. Claudin-10 deficiency also interfered with renal K^+ handling via an increase in respective FE values compared with controls (Table 1). Serum Na^+ and Cl^- levels and their renal FE excretion rates were not different between genotypes. In addition, serum creatinine and glomerular filtration rate (Table1) were not altered compared with controls. Taken together, these findings indicate that calcium deposition does not nonpecifically affect overall glomerular or tubular function.

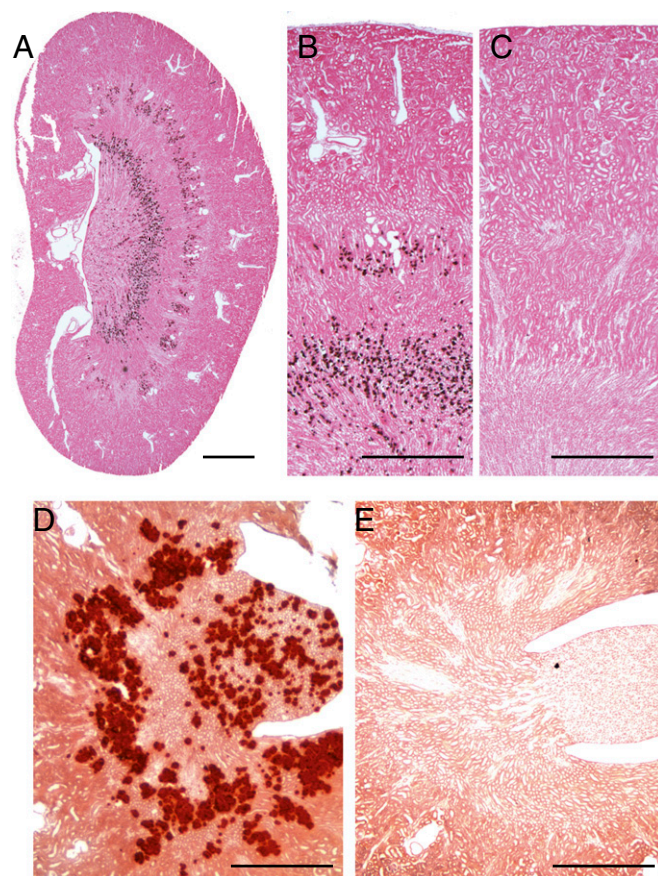**Fig. 2.** Histological analysis of kidneys revealing nephrocalcinosis in claudin-10–deficient kidneys (*A*, *B*, and *D*) compared with kidneys from control mice (*C* and *E*). Von Kossa (*A*–*C*) and alizarin red S (*D* and *E*) staining show a characteristic calcification pattern in both stripes of the outer medulla in cKO kidney sections. (Scale bars: 1 mm in *A*–*C*; 0.4 mm in *D* and *E*.)

Table 1. Serum and urine parameters in cKO and control mice

	Controls	cKO	n (control/cKO)
Serum parameters			
Na^+, mM/L	147.8 ± 1.1	148.4 ± 1.2	30/30
K^+, mM/L	6.1 ± 0.1	5.9 ± 0.1	30/30
Cl^-, mM/L	106.9 ± 0.8	106.4 ± 1.1	30/30
Ca^{2+}, mM/L	2.3 ± 0.0	2.1 ± 0.0***	29/30
Mg^{2+}, mM/L	1.1 ± 0.0	2.0 ± 0.1***	26/30
Phosphate, mM/L	2.8 ± 0.1	3.6 ± 0.2**	9/8
Urea, mM/L	22.7 ± 0.6	31.9 ± 1.0***	7/9
Creatinine, mM/L	0.015 ± 0.001	0.017 ± 0.001	16/17
Urine parameters			
FE_{Na}^+, %	0.4 ± 0.0	0.5 ± 0.0	16/17
FE_K^+, %	14.8 ± 0.7	17.4 ± 0.9*	16/17
FE_{Cl^-}, %	0.8 ± 0.1	0.7 ± 0.0	16/17
FE_{Ca}^{2+}, %	0.3 ± 0.0	0.2 ± 0.0*	16/17
FE_{Mg}^{2+}, %	8.9 ± 0.9	4.5 ± 0.3***	13/17
$FE_{phosphate}$, %	13.7 ± 0.8	15.0 ± 1.5	9/8
FE_{Urea}, %	41.8 ± 4.1	29.9 ± 2.0*	7/9
pH	6.3 ± 0.0	5.5 ± 0.0***	17/17
Osmolality, mOsm/kg	793 ± 44	419 ± 21***	9/8
Urine volume, mL	2.6 ± 0.2	5.2 ± 0.2***	30/30
Glomerular filtration rate, µL/min/g	8.9 ± 0.6	9.3 ± 0.5	17/17
Drinking volume, mL	1.3 ± 0.2	3.2 ± 0.5**	17/17

cKO animals are characterized by hypermagnesemia accompanied by reduced FE of Mg^{2+} and diuresis. Data are shown as mean ± SEM. n, number of experiments for control/cKO mice. *$P < 0.05$; **$P < 0.01$; ***$P < 0.001$.

Claudin-10 Deficiency in the TAL Alters Paracellular Permeability of Monovalent and Divalent Cations. The expression pattern of claudin-10 and the observed changes in urine and plasma electrolyte concentrations prompted us to test the electrophysiological properties of the TAL in freshly isolated tubules (Fig. 3). TALs of both genotypes showed typical lumen-positive, furosemide-inhibitable transepithelial voltage (V_{te}) (Fig. 3A). The 1.6-fold increase in V_{te} in cKO mice was accompanied by a 1.3-fold increase in transepithelial resistance (R_{te}), with no significant difference in short-circuit currents (I'_{sc}) (Fig. 3B). To gain further insight into the permeability properties of the TJs, we performed dilution potential and bi-ionic diffusion potential measurements in the continuous presence of furosemide (Fig. 3 C and D). The NaCl dilution potential was dramatically diminished in cKO mice (Fig. 3C, Left: −4.2 ± 1.7 mV in cKO mice vs. −23.2 ± 1.3 mV in controls). In addition, the bi-ionic diffusion potentials (luminal Na^+ against basolateral Mg^{2+} or Ca^{2+}) changed polarity in cKO tubules compared with controls (Fig. 3C, Right: 4.9 ± 1.0 mV in cKO mice vs. −7.4 ± 1.1 mV in controls for Mg^{2+} and 11 ± 1.5 mV in cKO mice vs. −0.7 ± 1.2 mV in controls for Ca^{2+}). The calculated relative permeabilities showed a decrease in P_{Na}/P_{Cl} accompanied by strong increases in P_{Mg}/P_{Na} and P_{Ca}/P_{Na} (P_x: permeability of the respective ion) (Fig. 3D). These findings suggest that the absence of claudin-10 alters the permeability sequence for different cations from monovalent to divalent.

Altered Renal Expression of Claudins and Distal Ion Transporters in *Cldn10*-Deficient Mice. Based on the hypermagnesemia and increased tubular absorption of Ca^{2+} and Mg^{2+} seen in *Cldn10*-deficient mice, we hypothesized that the defect of claudin-10 in the TAL might trigger compensatory reactions in the regulation of salt and water transport. The nephron segments distal to the TAL are of particular interest in the expression of genes involved in these compensatory mechanisms. Thus, we used qPCR to investigate expression changes of other renal claudins. We found that levels of *Cldn16* and *Cldn19* transcripts were increased by 1.6-fold and 1.7-fold, respectively (Fig. 4A). Remarkably, *Cldn14* transcript levels were dramatically increased, by more than 20-fold, in kidneys of cKO mice. In addition, expression of *Cldn11* (the renal function of which remains unknown) was reduced by 75%. The levels of *Cldn3* and *Cldn18* were similar in cKO mice and controls. We also detected changes in gene expression of distal nephron proteins involved in renal electrolyte and water transport (Fig. 4 and Table S1). Expression of genes involved in distal convoluted tubule (DCT) reabsorption of Ca^{2+} [*Calb1* (calbindin-D28k), *S100g*
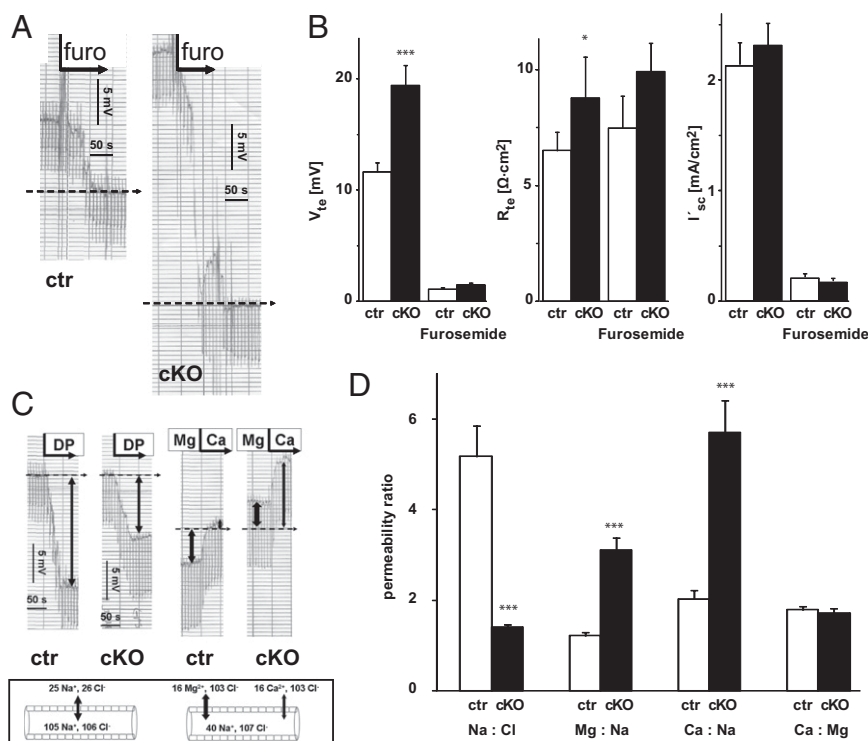
Fig. 3. Electrophysiological properties and permeability ratios of isolated perfused TAL in control and cKO mice. (A) Original chart recordings of furosemide-inhibitable lumen-positive V_{te} (continuous line). Voltage deflections are caused by current injections for the measurement of R_{te}. In the presence of luminal furosemide (furo), V_{te} drops to virtually 0 mV (dashed line). The respective change in V_{te} is larger in cKO TAL compared with control TAL. (B) Summarized data of V_{te}, R_{te}, and equivalent I'_{sc} under control conditions and in the presence of furosemide. cKO tubules exhibit higher voltage, higher resistance, and equal transport current. (C) Original traces of NaCl dilution potentials (Left) and bi-ionic diffusion potentials (Right), shown by the continuous line. Voltage deflections are caused by current injections. (Box) Schematic drawing indicating ion gradients across the tubular epithelium (luminal and basolateral ion activities, in mmol/L). The dashed line represents V_{te} at full inhibition of transcellular transport without paracellular ion gradients. cKO tubules show lower diffusion voltage and a strong shift of V_{te} to more positive values compared with control. (D) Relative ion permeabilities calculated from diffusion voltages. Absence of claudin-10 reduces Na^+ permeability in favor of Mg^{2+} and Ca^{2+} permeability. Data are shown as mean ± SEM. n = 22/15. *$P < 0.05$; ***$P < 0.001$.
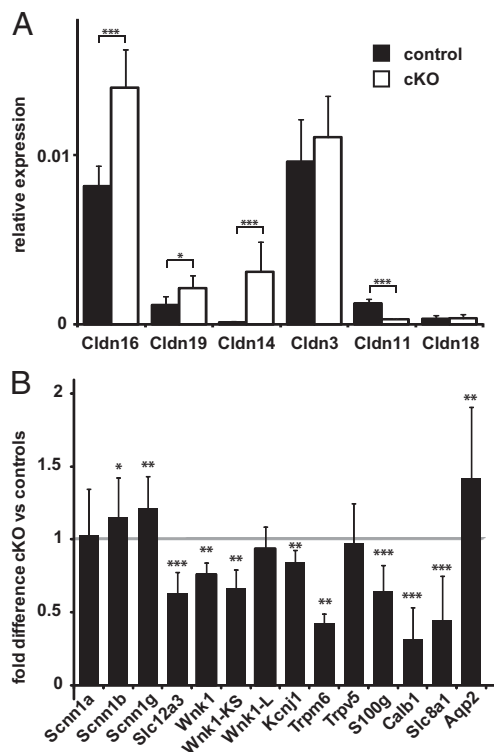
Fig. 4. Gene expression analysis of renal claudins (*A*) and representative renal ion transporters and channels (*B*) by real-time PCR. *Cldn10* deficiency results in differential gene expression of several genes. Values from cKO animals are shown relative to control mice (mean ± SEM). *Wnk1*, *Wnk1-KS*, *Kcnj1*, and *Trpm6*, n = 5/4; all other genes, n = 10/10. *P < 0.05; **P < 0.01; ***P < 0.001.

(calbindin-D9k), and *Slc8a1* (Na$^+$–Ca^{2+} exchanger)] and Mg^{2+} (*Trpm6*) was decreased in kidneys deficient in claudin-10. In turn, transcripts for aquaporin-2 (*Aqp2*), which promotes water conservation in the collecting ducts, and the β and γ subunits of epithelial sodium channel ENaC (*Scnn1b* and *Scnn1g*), responsible for electrogenic Na$^+$ absorption in the connecting tubules and collecting ducts, were expressed at higher levels in cKO mice. In contrast, the thiazide-sensitive NaCl cotransporter NCC (*Slc12a3*), the protein involved in NaCl absorption in the DCT, and the respective inhibitory, kidney-specific kinase-defective KS-WNK1 were expressed at lower levels in the cKO mice. Taken together, these data suggest specific compensatory alterations in components of both paracellular and transcellular renal ion transport mechanisms in mice deficient in claudin-10 in the TAL.

Phenotype in Claudin-10 Deficiency Originates from TAL Dysfunction. To test whether the observed phenotype of cKO mice originated from impaired transport processes in the TAL, we analyzed serum and urine parameters in mice given furosemide (Table 2). Analysis of the respective control and cKO mice without furosemide treatment confirmed the phenotype of hypermagnesemia and increased renal Mg^{2+} reabsorption in the cKO mice. In addition, urinary acidification, lower urine osmolality, increased FE$_{K+}$, hyperphosphatemia, and slight hypocalcemia appeared to be robust phenotypic features in cKO mice (Tables 1 and 2). Both cKO and control mice responded to i.p. injection of furosemide with impaired salt absorption in the TAL and increased urine production. In serum, furosemide treatment negated the differences in Ca^{2+} level, whereas hypermagnesemia remained unchanged.

In contrast, urinalysis demonstrated that the inhibition of TAL tubular transport by furosemide resulted in a completely different pattern of tubular Ca^{2+} and Mg^{2+} handling that identifies the TAL as the major nephron segment affected by claudin-10 deficiency. The lower or equal FEs of Mg^{2+} and Ca^{2+} in cKO

mice compared with controls without furosemide became higher FE values in the presence of furosemide, revealing the compensatory state of the nephron in cKO mice (Table 2).

Modest polyuria, as seen in the claudin-10–deficient mice, suggests a problem of urine concentration. We thus deprived animals of water to challenge their concentrating abilities (Table 3). Indeed, whereas control animals responded to water deprivation by producing significantly more concentrated urine, the cKO animals did not demonstrate an appropriate increase in urine concentration. Consequently, the serum levels of all measured electrolytes increased, owing to volume depletion. As shown previously, analysis of treatment groups without water deprivation has confirmed the phenotype of hypermagnesemia, increased renal Mg^{2+} reabsorption, urine acidification, lower urine osmolality, and hypocalcemia in cKO mice compared with controls.

Discussion

In contrast to channels and transporters involved in transcellular transports of ions in the TAL, the molecular components of the paracellular pathway in this tissue have not yet been characterized in full detail. In the present study, mice lacking claudin-10 in the TAL presented with disturbances in the homeostasis of Ca^{2+} and Mg^{2+} homeostasis, as evidenced by hypocalcemia, hypermagnesemia, hyperphosphatemia, and nephrocalcinosis. Based on our data and that of others, the claudin-10 isoform expressed in this nephron segment is claudin-10b (9, 17, 18). Accordingly, using the *ksp-cre* mouse line, we specifically ablated claudin-10b expression in the TAL, but did not alter expression of claudin-10a in the PCT, as demonstrated by immunohistology and qPCR (Fig. 1). Therefore, our cKO mouse line represents a unique model for investigating the specific functions of claudin-10 in TAL. We cannot rule out the possibility that claudin-10 is involved in transport processes in the other segments as well.

TAL salt transport is the driving force behind the urinary countercurrent concentrating system, generating the corticomedullary osmolarity gradient and energizing accumulation of urea in the renal medulla. Based on data identifying claudin-10 as a TJ protein serving in paracellular Na$^+$ transport (9, 17), we hypothesized that renal sodium reabsorption in the TAL of cKO mice might be disturbed. Indeed, the permeability for Na$^+$ in isolated TAL tubules was reduced fourfold. Given that transcellular transport in TAL, reflected by the equivalent short-circuit current, did not differ between genotypes, the impeded paracellular Na$^+$ passage led to an increased furosemide-inhibitable V$_{te}$. This effect was demonstrated by the almost twofold increased V$_{te}$ in the TAL of cKO mice compared with controls. A potentially reduced uptake of Na$^+$ in the TAL did not result in sodium loss, possibly owing to compensatory mechanisms in distal parts of the nephron. This assumption is supported by evidence indicating stimulation of salt and water absorption through enhanced expression of ENaC subunit transcripts, urine acidification, and increased renal K$^+$ excretion. Moreover, expression of *Aqp2* transcripts was enhanced and urea excretion was decreased, whereas serum values increased. In contrast, NaCl reabsorption in the DCT via the thiazide-sensitive protein NCC was down-regulated, reflecting the need for Na$^+$ reabsorption independent of Cl$^-$. But this compensation was not sufficient to counterbalance the water loss owing to the CKO's limited concentrating ability. Of note, Cl$^-$ excretion tended to be decreased in the cKO mice, indicating an apparent reciprocal effect on reabsorption of Na$^+$ and Cl$^-$. The concentrating defect became more prominent after water deprivation, which led to a hypovolemia in the cKO mice. An alternative explanation for the water loss in cKO mice is that nephrocalcinosis might have non-specifically affected the concentrating ability of the claudin-10–deficient kidney.

The elevated V$_{te}$ in the TAL resulted in an increased driving force for paracellular transport of cations in the TAL and increased reabsorption of Ca^{2+} and Mg^{2+} at the given TJ selectivity in cKO mice, which in turn led to hypermagnesemia and nephrocalcinosis. These alterations led to increased expression of *Cldn14*, which was identified as a negative regulator of the permeability formed by claudin-16 and claudin-19 in vitro and expressed under high

Table 2. Serum and urine parameters of control and cKO mice with and without furosemide treatment

	Without furosemide		With furosemide	
	Control	cKO	Control	cKO
Serum parameters				
Na^+, mM/L	152.3 ± 0.5	155.5 ± 0.9*	149.5 ± 0.50	151.1 ± 0.8
K^+, mM/L	5.0 ± 0.1	4.8 ± 0.2	4.9 ± 0.14	5.0 ± 0.2
Cl^-, mM/L	112.0 ± 0.5	111.3 ± 0.9	100.5 ± 0.71	97.9 ± 0.8*
Ca^{2+}, mM/L	2.3 ± 0.03	2.2 ± 0.02*	2.5 ± 0.04	2.5 ± 0.03
Mg^{2+}, mM/L	1.1 ± 0.03	1.9 ± 0.06***	1.3 ± 0.03	1.7 ± 0.04***
Phosphate, mM/L	2.5 ± 0.1	3.0 ± 0.1*	3.1 ± 0.2	3.3 ± 0.0
Creatinine, mM/L	0.015 ± 0.001	0.018 ± 0.001**	0.025 ± 0.001	0.031 ± 0.000**
Urine parameters				
FE_{Na+}, %	1.5 ± 0.1	2.0 ± 0.2*	10.1 ± 0.60	14.7 ± 3.1
FE_{K+}, %	21.6 ± 2.4	38.6 ± 4.0**	80.8 ± 7.76	156.6 ± 22.5*
FE_{Cl-}, %	2.4 ± 0.2	3.0 ± 0.3	17.7 ± 1.08	28.0 ± 5.7
FE_{Ca2+}, %	0.5 ± 0.1	0.5 ± 0.1	3.0 ± 0.40	15.6 ± 3.2**
FE_{Mg2+}, %	12.6 ± 1.4	8.9 ± 0.7*	26.1 ± 2.00	62.3 ± 9.5**
$FE_{phosphate}$, %	7.7 ± 1.4	10.8 ± 1.5	22.6 ± 3.67	60.5 ± 7.8**
pH	7.2 ± 0.2	5.9 ± 0.1**	6.9 ± 0.19	6.3 ± 0.1*
Osmolality, mOsm/kg	1,087 ± 53	536 ± 6**	478 ± 22	402 ± 6*
Urine volume, mL	0.6 ± 0.0	1.0 ± 0.1**	1.5 ± 0.16	2.2 ± 0.2*
Drinking volume, mL	0.5 ± 0.2	0.8 ± 0.2	0.8 ± 0.20	1.0 ± 0.1

Furosemide inhibits transcellular NaCl transport in TAL and thereby attenuates the driving force for paracellular cation reabsorption. The differential effect of furosemide in cKO mice unmasks hyperreabsorption of Ca^{2+} and Mg^{2+} in the TAL. Data are shown as mean ± SEM for n = 5–6 (without furosemide) and n = 5–8 (with furosemide) samples.*$P < 0.05$;**$P < 0.01$;***$P < 0.001$.

calcium loads (15). Interestingly, the different effects on plasma Mg^{2+} and Ca^{2+} levels reflect the different major reabsorption sites of these ions. Some 60% of the filtered Mg^{2+} is reabsorbed in the TAL, compared with only 20% of the filtered Ca^{2+} load (20). Ca^{2+} hyperreabsorption in TAL seems to be balanced by reduced (proximal and) distal tubular Ca^{2+} transport. This view is supported by the reduced expression of several genes involved in distal tubular transport of divalent cations. To our surprise, cKO mice had slightly but consistently lower serum Ca^{2+} concentrations. Ca^{2+} and Mg^{2+} act on the calcium-sensing receptor in the parathyroid gland (21), controlling the release of parathyroid hormone (PTH) (22). PTH in turn controls Ca^{2+}, phosphate, and vitamin D

metabolism to appropriately stabilize plasma Ca^{2+} levels. In a state of hypermagnesemia in cKO mice, this regulatory pathway may be stimulated by Mg^{2+} via the calcium-sensing receptor, preventing appropriate control of PTH release, a progressive decrease in serum phosphate, and normalization of serum Ca^{2+}.

The down-regulation of these alternative Mg^{2+} and Ca^{2+} uptake pathways became obvious when the TAL transport was blocked by furosemide. Furosemide treatment led to fivefold greater Ca^{2+} excretion and twofold greater Mg^{2+} excretion in cKO mice compared with furosemide-treated control mice. This phenotype may be related to the low expression of the genes involved in the distal reabsorption of divalent cations, which cannot be acutely restored

Table 3. Serum and urine parameters of control and cKO mice with and without access to water for 16 h

	Water		No water	
	Control	cKO	Control	cKO
Serum parameters				
Na^+, mM/L	152.8 ± 0.5	152.8 ± 0.6	154.2 ± 0.4	174.8 ± 1.1**
K^+, mM/L	4.6 ± 0.1	4.6 ± 0.1	4.5 ± 0.1	5.4 ± 0.2*
Cl^-, mM/L	114.5 ± 2.0	113.0 ± 0.9	113.0 ± 0.9	132.6 ± 1.7**
Ca^{2+}, mM/L	2.4 ± 0.01	2.1 ± 0.03**	2.4 ± 0.01	2.3 ± 0.03
Mg^{2+}, mM/L	1.2 ± 0.06	2.0 ± 0.12**	1.1 ± 0.06	2.8 ± 0.21**
Phosphate, mM/L	2.5 ± 0.1	2.8 ± 0.1*	2.7 ± 0.3	4.9 ± 0.5*
Creatinine, mM/L	0.017 ± 0.0	0.019 ± 0.0*	0.017 ± 0.0	0.031 ± 0.0*
Urine parameters				
FE_{Na+}, %	0.5 ± 0.0	0.6 ± 0.0	0.4 ± 0.0	0.6 ± 0.1
FE_{K+}, %	23.5 ± 2.3	28.6 ± 1.9	25.3 ± 2.1	44.1 ± 6.3
FE_{Cl-}, %	0.9 ± 0.1	0.8 ± 0.0	0.9 ± 0.1	1.0 ± 0.2
FE_{Ca}^{2+}, %	0.4 ± 0.2	0.1 ± 0.0	0.1 ± 0.0	0.1 ± 0.0
FE_{Mg2+}, %	12.0 ± 0.9	5.6 ± 0.4**	10.1 ± 1.5	4.3 ± 0.6*
$FE_{phosphate}$, %	19.2 ± 1.7	21.8 ± 2.4	20.3 ± 3.3	17.1 ± 0.9
pH	5.8 ± 0.1	5.0 ± 0.0**	5.4 ± 0.1	5.0 ± 0.1*
Osmolality, mOsm	860 ± 15	514 ± 18**	1610 ± 163	618 ± 13**
Urine volume, mL	2.1 ± 0.1	3.6 ± 0.7	1.1 ± 0.7	2.8 ± 0.2*
Drinking volume, mL	1.4 ± 0.2	2.7 ± 0.7		

Data are shown as mean ± SEM for $n \geq 4$ in each group.*$P < 0.05$;**$P < 0.01$.

PHYSIOLOGY

within the limited time of furosemide application. In contrast, furosemide has a very rapid effect on PTH secretion, possibly explaining the observed increase in FE of phosphate (23). The most prominent indicator of the elevated reabsorption of Ca^{2+} in TAL and hyperphosphatemia is the extensive nephrocalcinosis observed in cKO mice. The deposits are seen along the outer stripe of the outer medulla and in the inner stripe of the outer medulla at the transition to the inner medulla, in which the TAL is located and the hyperreabsorption of Ca^{2+} takes place.

The hyperreabsorption of divalent cations in mice deficient in claudin-10 is in opposition to the loss of divalent cations seen in mouse models of claudin-16 deficiency and in human patients with mutation in *CLDN16* or *CLDN19* (8, 11–14). This finding indicates that claudins in the TAL have functions that differentially affect paracellular cation transport in this segment. Mice deficient for claudin-10b in the TAL exhibit decreased permeability for Na^+ and increased permeability for Ca^{2+} and Mg^{2+}, whereas in mice with claudin-16 or claudin-19 deficiency, decreased sodium permeability in the TAL is paralleled by decreased reabsorption of Ca^{2+} and Mg^{2+} (24). Currently, we can only speculate on the molecular and biophysical implications of this finding. Recently, the presence of two pores of high and low capacity in the TAL has been suggested (25, 26). The function of the pore impaired by deletion of *Cldn10* would then mediate paracellular flux of Na^+, whereas the pore for Ca^{2+} and Mg^{2+} would be dependent on the presence of other claudins. However, claudins can form heterodimers, and the absence of one protein species may impact the expression of another (10). Moreover, claudins that are considered non–pore-forming may influence pore properties of renal TJs, as in the case of claudin-14. The increased expression of *Cldn14* in *Cldn10* cKO mice is in line with the recently proposed regulation of paracellular tranport of divalent cations. Thus, functional elucidation of the TJ complexes in the kidney remains a challenge. Clearly, mouse models with targeted disruption of components of the TJ, such as the model for claudin-10 described here, are critical to resolving the molecular mechanism underlying paracellular ion transport and its relevance for renal (patho)physiology.

Materials and Methods

Antibodies. Primary antibodies were rabbit anti-claudin-10, mouse anti-occludin, mouse anti–ZO-1 (Life Technologies), guinea pig anti-NKCC2, mouse anti-NHE3 (Chemicon), rabbit anti–claudin-16, rabbit anti–claudin-19 (15), and rabbit anti-actin (Sigma-Aldrich). Secondary antibodies were coupled to Alexa Fluor 488, Alexa Fluor 555 (Life Technologies), or HRP (Sigma-Aldrich).

Physiology. All experimental procedures in mice were approved by the Institutional Animal Care and Use Committee of the Max Delbrueck Center (Berlin) and conducted in accordance with guidelines for proper conduct of animal experiments. Urine samples were collected from mice placed in metabolic cages for 17 h. Blood sampling was performed by retro-orbital puncture. Ion concentrations in urine and serum were measured using standard clinical analysis or colorimetric detection (Quantichrom Magnesium Assay Kit; Gentaur).

Furosemide (Sigma-Aldrich) was dissolved in DMSO, diluted in saline, and injected i.p. at a dose of 40 mg/kg. Mice were immediately placed in metabolic cages, and urine was collected for 4 h. Mice were killed after blood sampling.

For the water-deprivation studies, water supply was removed from the cages in the morning. After 8 h, the mice were placed in metabolic cages, and urine was collected overnight. After 17 h, blood sampling was performed, after which the mice were killed.

Renal Tubule Perfusion. Perfusion and transepithelial measurements in freshly isolated mouse TAL segments were performed as described previously (2). Tubules were isolated mechanically and transferred into the bath on a heated microscope stage. Tubules were held and perfused using a concentric glass pipette system. The perfusion pipette was double-barreled, with an outer diameter of 10–12 μm. Barrel 1 was used for perfusion, fluid exchange, and voltage measurement, and barrel 2 was used for constant current injection (13 nA). Cable equations as described previously (2) were used to calculate transepithelial resistance, R_{te}. Equivalent short-circuit current I_{sc} was calculated from R_{te} and V_{te} according to Ohm's law. Perfusion rates were 10–20 nL/min. The bath was thermostat-controlled at 37 °C, and continuous bath perfusion at 3–5 mL/min was maintained by gravity perfusion. The compositions of the solutions used are specified in Table S2.

Transcellular transport was measured under symmetrical luminal and basolateral perfusion with control solution (Ctrl) and after luminal application of 50 μmol/L of furosemide in Ctrl. In the continuous presence of luminal furosemide, basolateral and/or luminal fluids were replaced by modified solutions. For the dilution potential and the calculation of P_{Na}/P_{Cl}, NaCl was diluted isosmotically at the basolateral side (30 Na). Considering different activity coefficients for monovalent and divalent ions, 55 Na was applied luminally for bi-ionic diffusion potential measurements. Bi-ionic diffusion potentials were then measured after basolateral application of 72.5 Mg and 72.5 Ca, respectively. Permeability ratios were calculated according to the method of Günzel et al. (17)

1. Seyberth HW, Schlingmann KP (2011) Bartter- and Gitelman-like syndromes: Salt-losing tubulopathies with loop or DCT defects. *Pediatr Nephrol* 26:1789–1802.
2. Greger R (1981) Cation selectivity of the isolated perfused cortical thick ascending limb of Henle's loop of rabbit kidney. *Pflugers Arch* 390:30–37.
3. Furuse M (2010) Molecular basis of the core structure of tight junctions. *Cold Spring Harb Perspect Biol* 2:a002907.
4. Mineta K, et al. (2011) Predicted expansion of the claudin multigene family. *FEBS Lett* 585:606–612.
5. Colegio OR, Van Itallie CM, McCrea HJ, Rahner C, Anderson JM (2002) Claudins create charge-selective channels in the paracellular pathway between epithelial cells. *Am J Physiol Cell Physiol* 283:C142–C147.
6. Piontek J, et al. (2008) Formation of tight junction: Determinants of homophilic interaction between classic claudins. *FASEB J* 22:146–158.
7. Kiuchi-Saishin Y, et al. (2002) Differential expression patterns of claudins, tight junction membrane proteins, in mouse nephron segments. *J Am Soc Nephrol* 13:875–886.
8. Konrad M, et al. (2006) Mutations in the tight-junction gene claudin 19 (CLDN19) are associated with renal magnesium wasting, renal failure, and severe ocular involvement. *Am J Hum Genet* 79:949–957.
9. Van Itallie CM, et al. (2006) Two splice variants of claudin-10 in the kidney create paracellular pores with different ion selectivities. *Am J Physiol Renal Physiol* 291:F1288–F1299.
10. Hou J, et al. (2009) Claudin-16 and claudin-19 interaction is required for their assembly into tight junctions and for renal reabsorption of magnesium. *Proc Natl Acad Sci USA* 106:15350–15355.
11. Simon DB, et al. (1999) Paracellin-1, a renal tight junction protein required for paracellular Mg2+ resorption. *Science* 285:103–106.
12. Hou J, et al. (2007) Transgenic RNAi depletion of claudin-16 and the renal handling of magnesium. *J Biol Chem* 282:17114–17122.
13. Himmerkus N, et al. (2008) Salt and acid-base metabolism in claudin-16 knockdown mice: Impact for the pathophysiology of FHHNC patients. *Am J Physiol Renal Physiol* 295:F1641–F1647.
14. Will C, et al. (2010) Targeted deletion of murine Cldn16 identifies extra- and intra-renal compensatory mechanisms of Ca2+ and Mg2+ wasting. *Am J Physiol Renal Physiol* 298:F1152–F1161.
15. Gong Y, et al. (2012) Claudin-14 regulates renal Ca++ transport in response to CaSR signalling via a novel microRNA pathway. *EMBO J* 31:1999–2012.
16. Thorleifsson G, et al. (2009) Sequence variants in the CLDN14 gene associate with kidney stones and bone mineral density. *Nat Genet* 41:926–930.
17. Günzel D, et al. (2009) Claudin-10 exists in six alternatively spliced isoforms that exhibit distinct localization and function. *J Cell Sci* 122:1507–1517.
18. Ohta H, Adachi H, Takiguchi M, Inaba M (2006) Restricted localization of claudin-16 at the tight junction in the thick ascending limb of Henle's loop together with claudins 3, 4, and 10 in bovine nephrons. *J Vet Med Sci* 68:453–463.
19. Shao X, Somlo S, Igarashi P (2002) Epithelial-specific Cre/lox recombination in the developing kidney and genitourinary tract. *J Am Soc Nephrol* 13:1837–1846.
20. Quamme GA (1997) Renal magnesium handling: New insights in understanding old problems. *Kidney Int* 52:1180–1195.
21. Brown EM, et al. (1993) Cloning and characterization of an extracellular Ca(2+)-sensing receptor from bovine parathyroid. *Nature* 366:575–580.
22. Ho C, et al. (1995) A mouse model of human familial hypocalciuric hypercalcemia and neonatal severe hyperparathyroidism. *Nat Genet* 11:389–394.
23. Haas JA, et al. (1977) Phosphaturic effect of furosemide: Role of PTH and carbonic anhydrase. *Am J Physiol* 232:F105–F110.
24. Hou J, Goodenough DA (2010) Claudin-16 and claudin-19 function in the thick ascending limb. *Curr Opin Nephrol Hypertens* 19:483–488.
25. Van Itallie CM, et al. (2008) The density of small tight junction pores varies among cell types and is increased by expression of claudin-2. *J Cell Sci* 121:298–305.
26. Günzel D, et al. (2009) Claudin function in the thick ascending limb of Henle's loop. *Ann N Y Acad Sci* 1165:152–162.